Pergamon

Journal of Structural Geology, Vol. 18, Nos 2/3, pp. 249 to 263, 1996

0191-8141/96 $15.00+0.00

0191-8141(94)E00090-9

High resolution fault displacement mapping from three-dimensional seismic data: evidence for dip linkage during fault growth

C. S. MANSFIELD and J. A. CARTWRIGHT

Department of Geology, Imperial College of Science, Technology and Medicine, Prince Consort Road, London SW7 2BP, U.K.

(*Received* 30 *January* 1995; *accepted in revised form* 5 *July* 1995)

Abstract—Detailed mapping using high resolution three-dimensional seismic data has revealed a number of sub-horizontal anomalies in the distribution of vertical displacement (throw) on the planes of growth faults in the Gulf of Mexico. Recognition of these anomalies is highly sensitive to the interval at which the fault displacements are sampled, because they represent local decreases in throw which are confined to small, discrete parts of the fault planes. The distribution of the anomalies is inconsistent with model displacement fields of quasi-elliptical concentric contours and is therefore incompatible with models of fault growth by uniform slip distribution and radial tip-line propagation. An alternative model is proposed, whereby the evolution of a fault plane is established by the propagation and linkage of precursor fault segments in the dip direction—'dip linkage'. Overlap and linkage of fault tips in the dip direction results in relay structures that are sub-parallel to fault strike and therefore displacement minima that are sub-horizontal on normal and thrust faults. However, since they are orthogonal to the main slip direction on the fault, these structures have a low preservation potential and are therefore unlikely to be well resolved on cross-sectional seismic profiles.

INTRODUCTION

Mapping fault displacement distributions is a relatively new technique that is increasingly being adopted as an aid in solving problems of subsurface fault correlation (Freeman *et al.* 1990). Many previous studies (Rippon 1985, Walsh & Watterson 1987, 1988, 1991, Chapman & Meneilly 1990, 1991, Petersen *et al.* 1992, Clausen & Korstgard 1994) have described broadly systematic fault displacement distributions that are claimed to be consistent with the model displacement field of an 'ideal, isolated blind fault' (Watterson 1986, Barnett *et al.* 1987). In this model, an arrangement of quasi-elliptical, concentric contours indicates a smooth decrease in displacement towards the tip-line from a single maximum at the centre of the fault plane. Incremental growth of the fault structure, either by earthquake rupture or stable sliding, is then argued to occur as a uniform radial propagation of the other tip-line driven by a systematic distribution of slip across the entire fault surface. Fault plane dimensions are at all times proportional to the maximum displacement on the fault, in a manner prescribed by a scaling equation (Watterson 1986).

Attention has recently been drawn, however, to the role of linkage between faults as a key element of fault lengthening in the growth of much larger fault structures (Segall & Pollard 1980, Ellis & Dunlap 1988, Martel *et al.* 1988, Peacock & Sanderson 1991, 1994, Dawers *et al.* 1993, Martel & Pollard 1993, Scholz *et al.* 1993, Trudgill & Cartwright 1994). Field studies in particular have described anomalous displacement distributions in the regions surrounding branch lines and relay structures along fault strike (Walsh & Watterson 1990, 1991, Peacock & Sanderson 1991, 1994, Trudgill & Cartwright 1994). These anomalous patterns are zones of locally high displacement gradient, often with values several times greater than the general displacement gradient over the rest of the fault surface. They consequently represent departures from the smooth distribution of a single, isolated fault and develop as a result of overlap and linkage between the tip regions of neighbouring faults as a relay structure is established (Peacock & Sanderson 1991). In cases where it has been possible to measure displacement distributions across regions of linkage between normal faults, the anomalies have been shown to be elongated sub-vertical zones, i.e. the long axes of the anomalies are sub-parallel to the fault slip vector (Walsh & Watterson 1991, Childs *et al.* 1993, 1995). This is consistent with the geometry of relay structures as being the product of linkage in the strike direction of the fault.

The aim of this paper is to present evidence that displacement anomalies on normal faults can also be found with their long axes oriented parallel to fault strike, i.e. orthogonal to the slip direction. Detailed displacement mapping on growth faults in the Gulf of Mexico, using a high resolution, three-dimensional seismic data set, shows that these anomalies can be consistently and accurately mapped, provided that there is a sufficiently high sampling density of displacements over the fault planes and that there is sufficient lateral and vertical resolution to allow for a precise definition of stratal relationships. The paper concludes with a discussion of possible explanations for the origin of these

anomalies, in the light of published examples of similar observations described from fault mapping in the field and from fault interpretations using seismic data.

GEOLOGICAL SETTING

The data set used in this study is part of a high resolution, three-dimensional seismic survey provided by GECO–PRAKLA. Located offshore Louisiana in shallow water (Fig. 1), the survey area covers a part of the continental margin that is dominated by a thick, mixed siliciclastic sequence of deltaic and pro-deltaic sediments of predominantly Late Cenozoic age, overlying Early Cenozoic slope and basin plain shales and Mesozoic evaporites (Murray 1951, Burgess 1976, Jackson & Galloway 1984). Gravitational collapse during progradation of deltaic sequences across much of the present day shelf region of the Gulf of Mexico has resulted in the development of an extensive series of growth faults (Jackson & Galloway 1984). In the region covered by the survey (Fig. 1), the fault structure is transitional between the two major fault trends present along the northern coast of the Gulf of Mexico (Reymond & Stampfli 1994), one set being approximately E–W and the other approximately NE–SW.

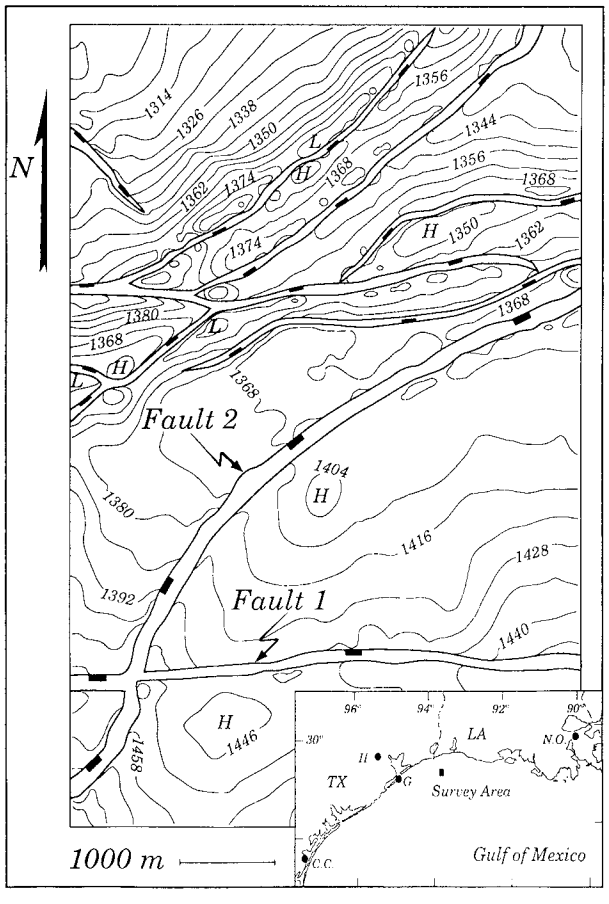

Fig. 1. Two-way travel time contour map of an intermediary level horizon interpreted from the seismic data. Survey dimensions are approximately 5 × 10 km and the contour interval is 6 ms. The labelled faults, 1 and 2, are selected for discussion of their displacement distributions; see text. Location map of the survey area is inset; TX = Texas, LA = Louisiana, CC = Corpus Christi, G = Galveston, H = Houston, NO = New Orleans.

The alternating sands, silts and clays of the deltaic deposits are expressed in the seismic data as a highly reflective sequence, with good lateral continuity (Fig. 2). The seismic data have been well migrated and consequently the positions of fault planes can be reliably interpreted, even in the deepest parts of the data set at 4000 ms two-way travel time (TWTT). The clarity of fault definition illustrated in Fig. 2 is typical of seismic profiles across the entire survey area. The faults exhibit marginally listric geometries in the deepest parts of the data set, becoming sub-vertical near their well-defined upper tips. Maximum fault throws vary considerably from one structure to another, the largest recorded being 160 ms one-way travel time on Fault 2 (Fig. 1). Using an average velocity of 3500 m s^{-1} over the entire depth range of the fault this corresponds to a throw of 560 m.

A thickening of strata from footwall to hangingwall, recording fault growth contemporaneous with sediment deposition, is indicated by the seismic data at most intervals across the planes of all of the faults in the survey area. Expansion ratios (downthrown thickness divided by upthrown thickness; Thorsen 1963) as great as 10 have been recorded across growth faults in the Gulf of Mexico, but maximum values across these relatively small faults are on average about 1.1, with a maximum value of 2.7 recorded over a limited stratigraphic interval.

DISPLACEMENT MAPPING

Fault interpretation and displacement mapping were carried out on a work-station, using Landmark seismic interpretation software. Since the faults trend subparallel to the basin margin and are therefore likely to have exhibited predominantly dip-slip displacement, and since the degree of curvature of the faults with depth is minimal (Fig. 2), then it was assumed that fault throw could safely be taken as a proxy for displacement. Values were measured by taking a series of strike-normal profiles across each of the faults at 50 m intervals and recording the TWTTs of reflections from the footwall and hangingwall cut-offs of selected horizons at discrete locations down the fault planes, approximately every 25–50 ms. To minimize spatial distortion of the distributions resulting from curvature of the fault planes along strike, the data were then projected onto strike-parallel vertical planes for contouring.

The only error in the calculated throw values arises from the accuracy with which the TWTTs could be measured from the peaks or zero crossings of the seismic reflections at each of the sample points on the faults. This is estimated to be ± 1 ms, i.e. approximately 4 m. However, an uncertainty in the positions of stratal terminations does introduce a second minimal error, associated with the position in depth of the recorded

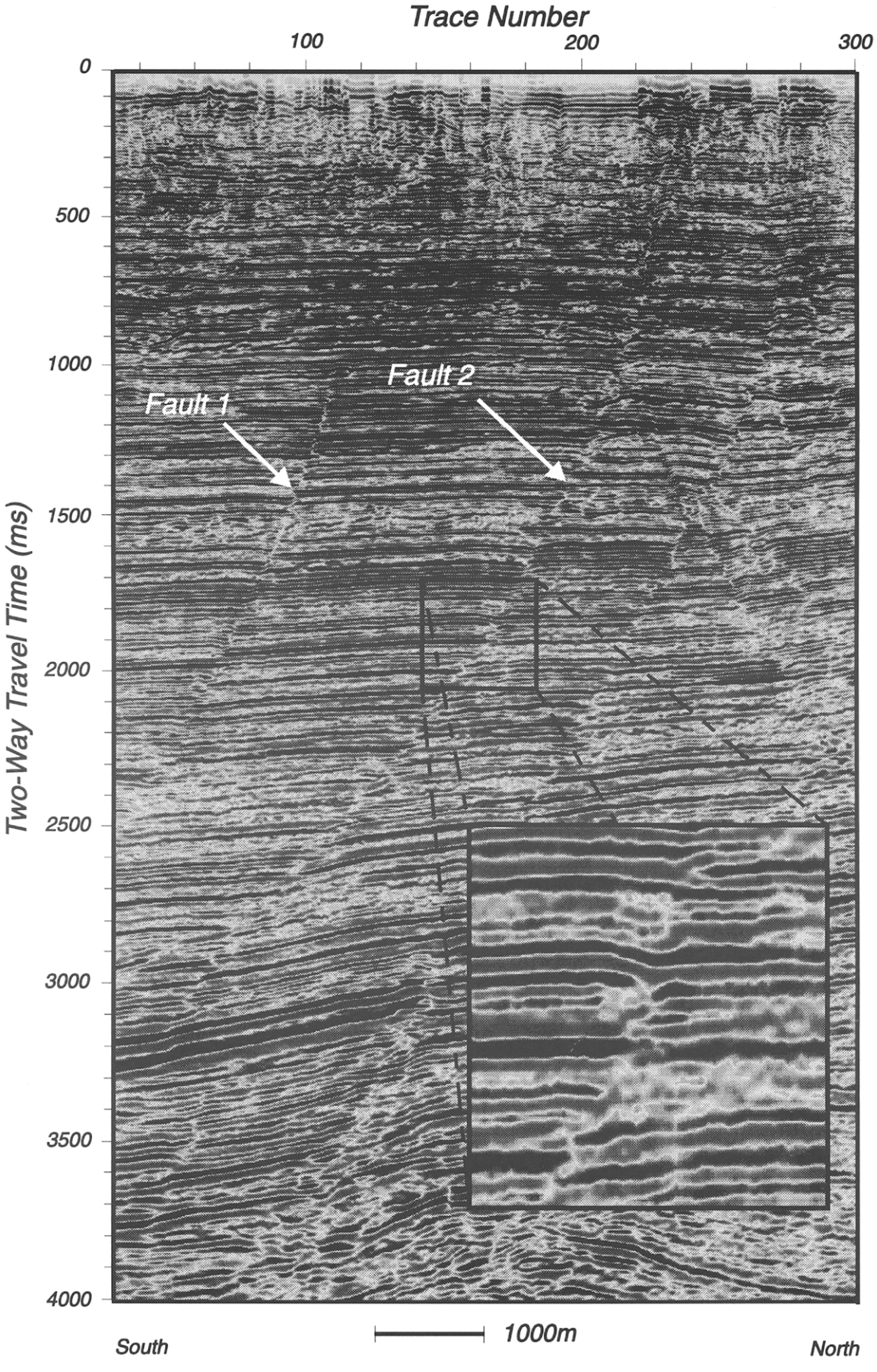

Fig. 2. Seismic cross-section showing fault structure in the southern half of the survey area. Inset section shows the detail of folding adjacent to one of the fault planes. Assuming an average velocity of 3500 m s^{-1} for the entire interval, vertical exaggeration is approximately 1.5.

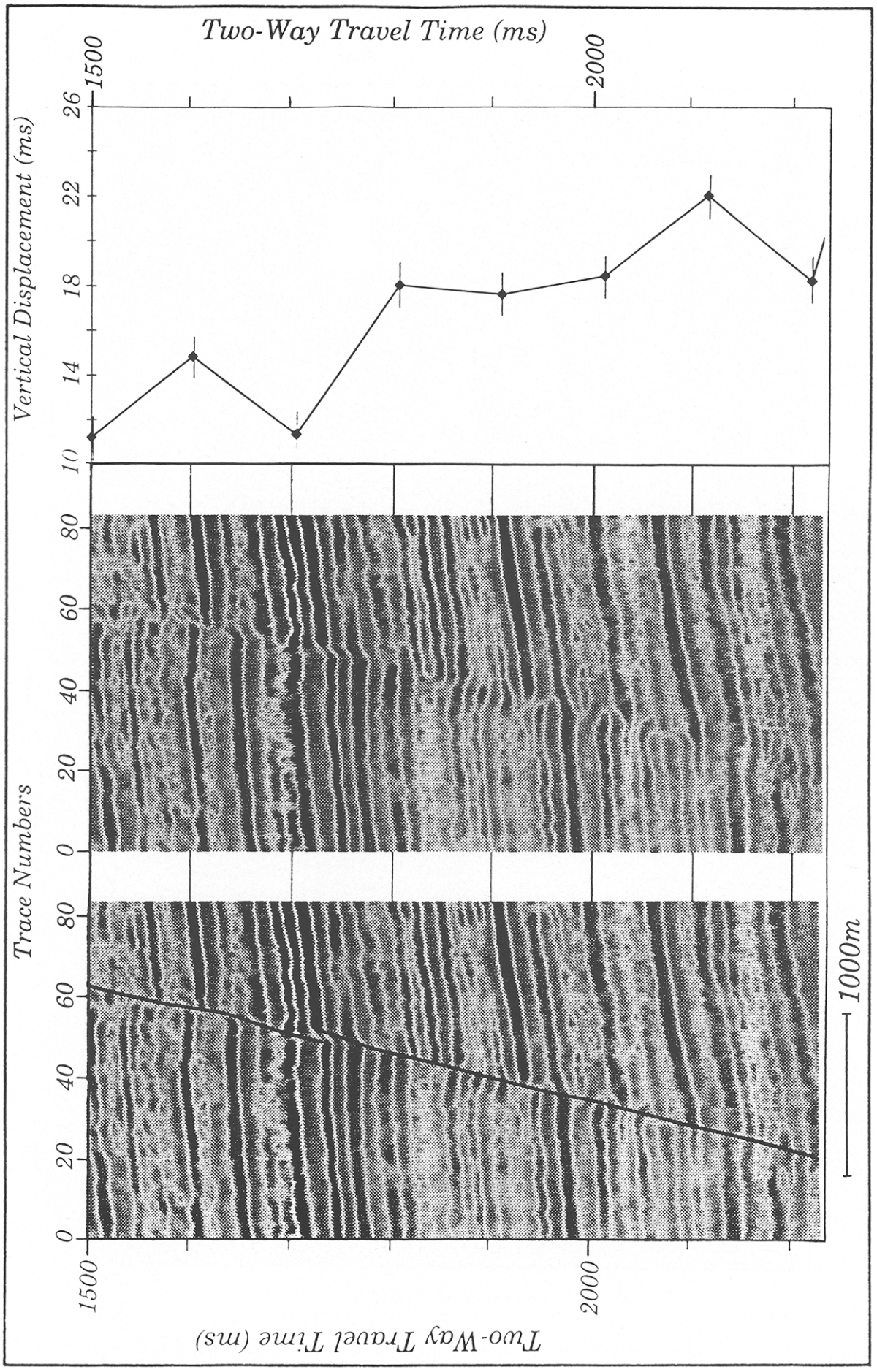

Fig. 10. Composite diagram showing a correlation of one of the recorded throw minima with a dip-direction relay structure interpreted from the seismic data. Rotation of bedding within the overlap zone is clearly apparent, separating two fault segments that within the resolution of the seismic data appear not to be linked. A decrease of displacement on both fault segments towards their respective tips results in a composite minimum being recorded.

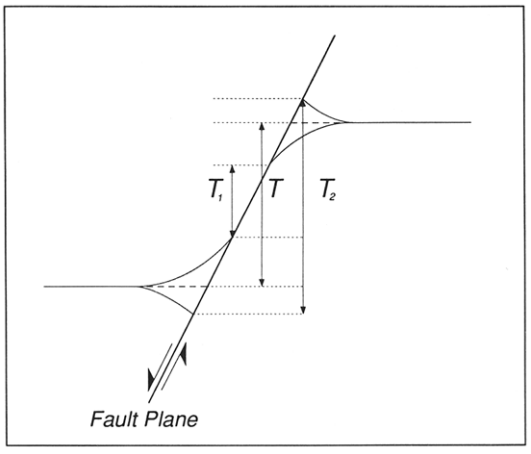

Fig. 3. Illustration showing how corrections for stratal folding adjacent to the fault planes were applied to the measurements of throw. In each case, corrections to true throw, T, were made by either adding or subtracting the proportions of fault throw accounted for by the deflection of bedding to the recorded measurements T_1 and T_2, respectively.

displacements. This is a function of the frequency content of the seismic data and is estimated in this case to be approximately equivalent to ±12 m.

All of the fault displacement fields have been modified by gentle folding of wall rock adjacent to the fault planes. This folding is developed in both the footwalls and the hangingwalls, and is well defined by the seismic data (Fig. 2). The deformation represents only a small proportion of the fault displacement at any location, but is highly variable both in magnitude and in style, accounting for up to 11 ms deflection of the bedding across zones stretching up to 500 m from some of the largest fault planes. It was therefore necessary to correct for this local perturbation of the displacement fields, using the technique employed by Chapman & Meneilly (1991), on a sample-by-sample basis (Fig. 3).

RESULTS

Displacement patterns

The distribution of throw has been mapped across most of the faults in the survey area. Many of the maps, however, are complicated by numerous intersections with neighbouring faults. Therefore, the results of displacement mapping are illustrated with reference to the two faults exhibiting the least number of intersections. They are the E–W striking fault in the southernmost part of the survey area (Fault 1) and the large arcuate fault in the middle of the survey area (Fault 2), as indicated in Fig. 1. The structure of the two faults is not known beyond the limits of the survey area.

The patterns of throw distribution on Faults 1 and 2 are expressed as contours of one-way travel time (OWTT), in ms, in Fig. 4. Both are typical of the distributions recorded on all the mapped faults. The distributions are bounded in each case laterally by the edges of the data set, at the base by a lower limit of measurement and at the top by an upper tip-line. The latter represents a zero displacement contour defined by the limit of displacement that can be resolved from the seismic data, estimated in this case to be no more than 12 m.

The contour pattern on Fault 1 (Fig. 4a) indicates a general increase in throw with depth towards three local maxima at points A, B and C, located close to the deepest imaged parts of the fault. The steep plunge of contours at the eastern end of the fault indicate a decrease in throw in this direction, whilst a local decrease in throw has also been recorded coincident with the oblique line of intersection with Fault 2. Apart from this, there are no other intersection relationships with, or apparent influence from, neighbouring faults. Locally, however, erratic contours punctuated by numerous small maxima and minima represent potentially significant departures from a smooth, idealized distribution.

The pattern of throw distribution on Fault 2 (Fig. 4b) is similarly complex. Within the survey limits, this fault has a greater surface area than Fault 1 and larger displacements. None the less, many comparable local anomalies are apparent in the throw distribution. The intersection with Fault 1 is indicated as a sub-vertical line at the southwestern end of the fault, adjacent to which there is a perturbation of the local displacement field similar to that associated with the line of intersection on Fault 1 (Fig. 4a). However, other, sub-horizontal, intersection lines indicated at the northeastern end of the fault have a much less pronounced effect on the contour pattern as they lie sub-parallel to the contour trend. A larger number of maxima and minima, with greater magnitude, have also been recorded, particularly along the deepest parts of the fault. Three local highs (A, C and F) and three lows (B, D and E), well defined close to the deepest limits of measurement, indicate that the distribution of throw is complex over the very deepest parts of the fault plane.

The small contour irregularities and local maxima and minima in the throw distributions described above appear to be genuine, resulting from local influences that are limited, both in dimension and magnitude. The sampling interval at which displacements are recorded governs the resolution of the final mapped distribution and therefore maintaining a consistently high sampling density is absolutely vital for recognizing the smallest and most subtle local displacement patterns. The importance of this is demonstrated in Fig. 5, which illustrates the differences in resolved throw distributions on Fault 1 derived from sample profiles at different spacings.

At a spacing of 1000 m, the distribution is similar to that predicted for the upper parts of the model of an ideal, isolated blind fault (Watterson 1986, Barnett *et al.* 1987). Smooth, gently arcuate contours with only very mild local gradients represent a uniform and systematic increase in displacement with depth. The wide profile spacing means that the mapping has failed to resolve any

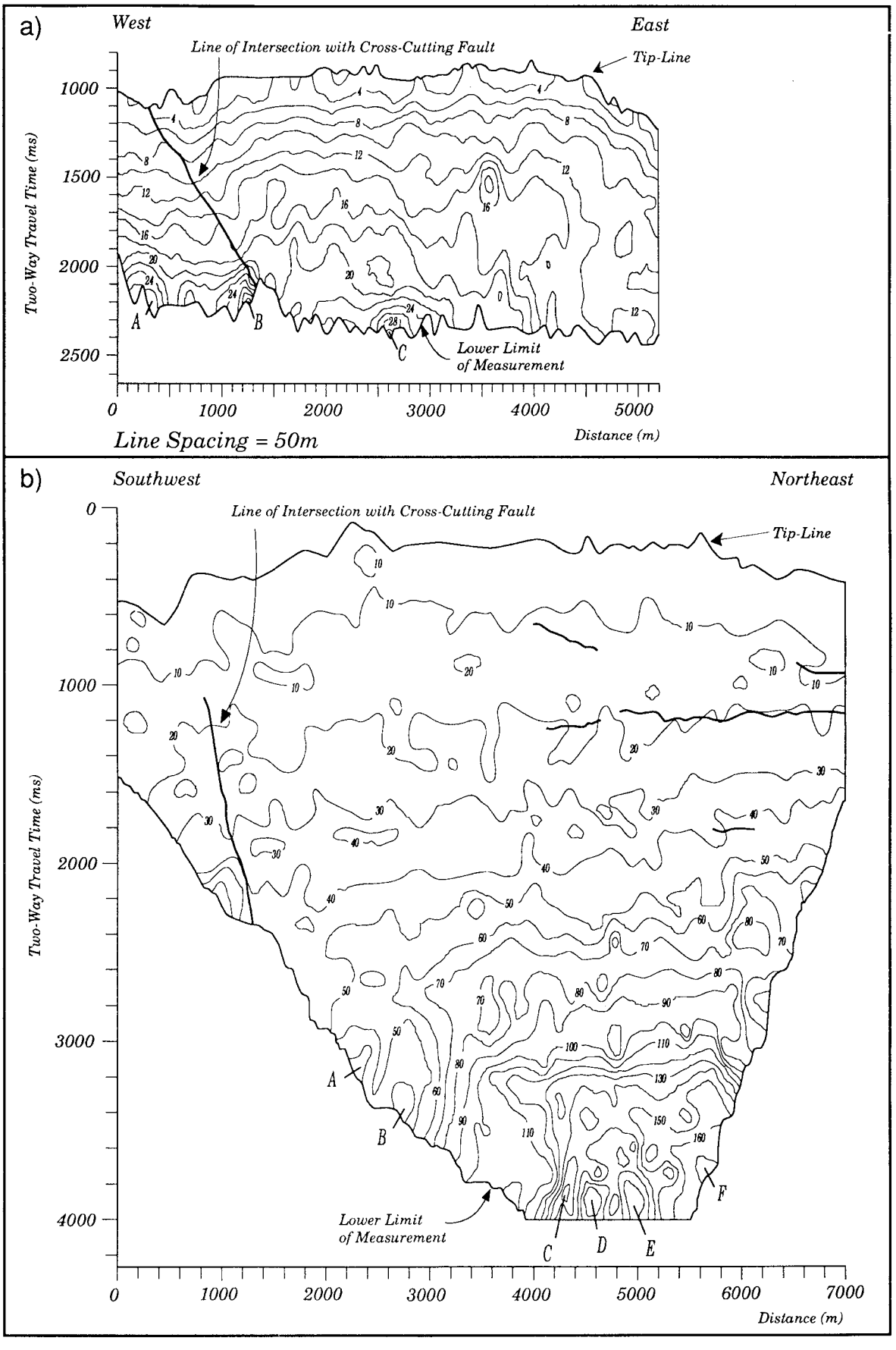

Fig. 4. Vertical strike projections of the distribution of vertical displacement (throw) on (a) Fault 1; (b) Fault 2. The distributions are defined from 1384 and 2319 discrete throw measurements respectively and are contoured in ms, OWTT. Throw on the deepest parts of both faults is characterized by numerous local maxima and minima, labelled A–F; see text. Lines of intersection with neighbouring faults are shown as bold, oblique and sub-horizontal lines, cross-cutting the contours. The faults are plotted at the same scale, with no vertical exaggeration.

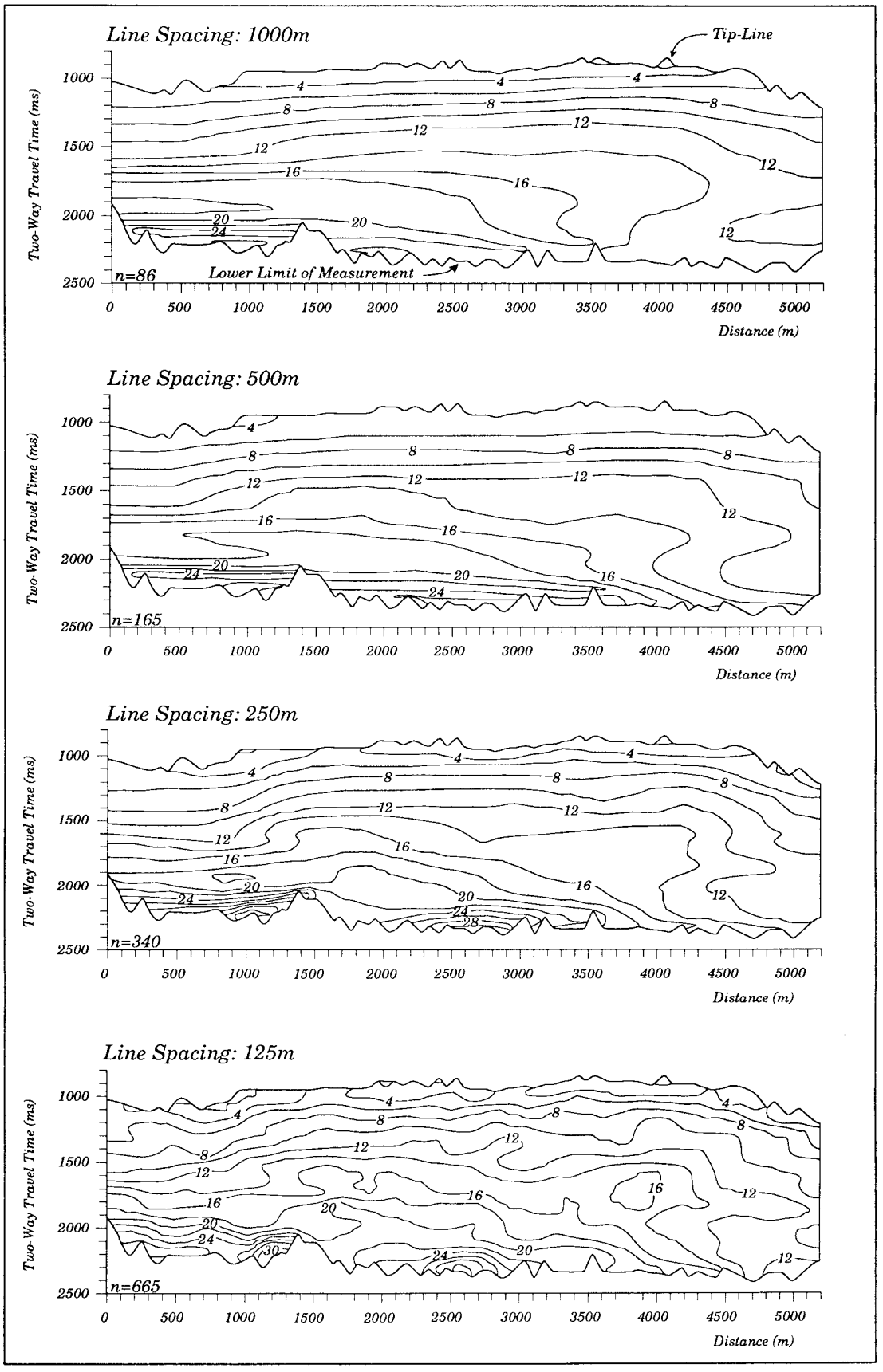

Fig. 5. A series of maps showing the distributions of throw over Fault 1 derived from sample profiles at different spacings. Successively greater complexities in the throw distributions are indicated by the contour patterns as a greater number of the small, local distributions are resolved at ever closer sample profile spacings. The number of discrete sample points used for contouring is indicated in each case.

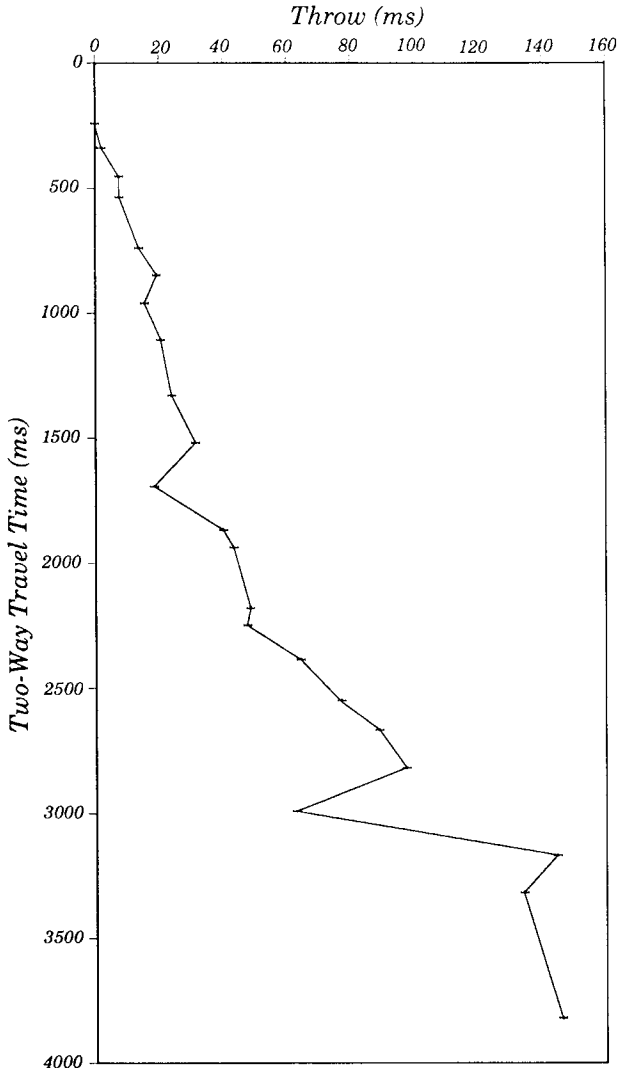

Fig. 6. An example profile of throw recorded from midway along Fault 2, defined in this case from 23 discrete measurements. The observed local throw minima are characteristic of sample profiles across all of the mapped faults. Estimated measurement error (± 1 ms) indicated at each sample point is clearly unable to account for most of these.

of the local, high frequency throw variations. However, with a reduction in the profile spacing, a greater proportion of the small, local displacement patterns are resolved and the contours reflect an increasingly complex throw distribution. Therefore, it is evident from this comparison that failing to select a sampling interval of sufficient density will result in a failure to identify anomalous distributions of throw.

Despite the high sampling density and clarity of the seismic data, no systematic pattern is apparent in the arrangement of the throw anomalies. However, many are small and of low amplitude, so that their definition and resolved spatial extent are particularly susceptible to aliasing by the chosen contouring interval. Therefore, the irregularities in the throw distributions and the nature of some of the smallest anomalies are more clearly seen in the recorded throw profiles. One example profile, taken from midway along Fault 2, is presented as Fig. 6. It shows that, although there is a general increase in throw with depth, there are also a number of localities at which there is a decrease in throw with depth, i.e. a local negative throw gradient. By plotting these points of negative throw gradient on a vertical strike plane for each of the faults, a clearer pattern in the anomalies of throw can be observed (Fig. 7). This approach overcomes the limitations of contouring resolution as it is sensitive only to the sign of the gradient rather than the absolute value of the throw. The regions of negative throw gradient can be identified as a series of small, closed contours that reflect the complexities seen in the original plots of throw distribution. The most striking feature of the displays is, however, the arrangement of some of the anomalies as sub-horizontal, semi-continuous bands distributed over the fault plane surfaces.

Effects of differential compaction and changes in seismic interval velocity

The local throw minima defined by these areas of negative displacement gradient reach magnitudes as great as 16 ms OWTT, much larger than the estimated measurement precision (± 1 ms), so they cannot be artefacts arising from resolution limitations in the methodology. Consequently, they either reflect a real variability in the throw distributions of the faults or, alternatively, are only apparent anomalies, resulting either from variations in seismic interval velocity or from the influence of differential compaction between correlative sedimentary units in the footwalls and hangingwalls.

The effects of differential compaction can be explained with reference to a buried, single layer in a hypothetical multi-layer medium. If the medium is unfaulted, then compacting any single layer results in an increase in the depth of burial for all overlying units. Where the medium is faulted, it follows that if the compaction is greater in the hangingwall than in the footwall then there will be a net increase in throw across the fault at all levels above (Fig. 8). Assuming a previously uniform increase of throw with depth (curve A), then if the differential compaction is substantial enough to increase the throw at the top of the compacting layer to a value greater than the throw at its base, a local decrease in throw will be generated (curve B).

Contrasts in seismic interval velocities, resulting either from differential compaction or changes in lithology across a fault, may generate apparent anomalies, and enhance or obscure existing anomalies, depending on the magnitude and the polarity of the contrast. For example, a higher velocity in the hangingwall unit of any correlative sedimentary sequence across a fault will result in a decrease in the associated travel time to the base of that unit. An erroneously low value of throw will then be apparent in the seismic data at that point on the fault. If the magnitude of the velocity contrast is great enough, relative to over- and underlying layers, then a local throw minimum may be recorded.

Therefore, using published burial curves (Magara

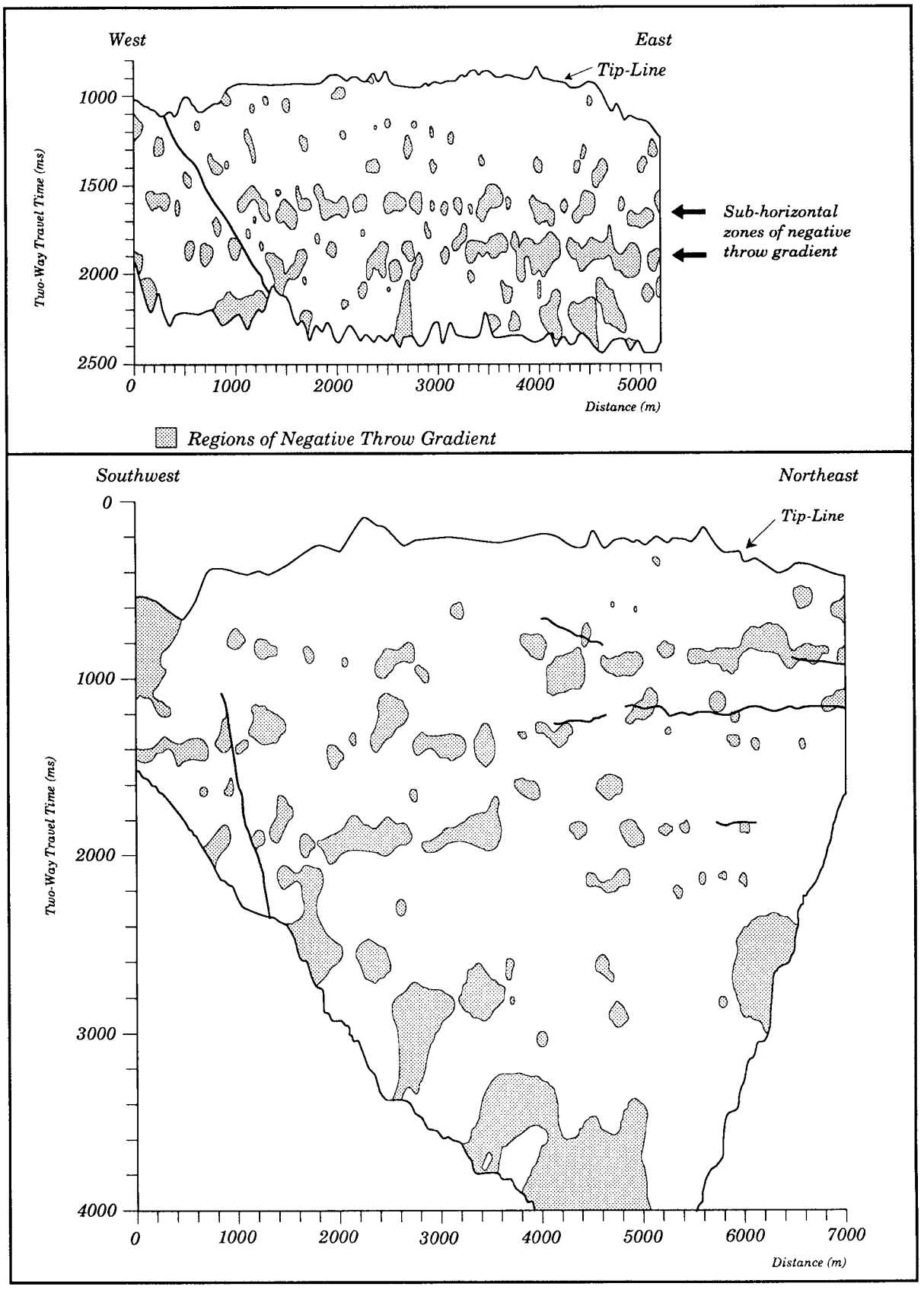

Fig. 7. Vertical strike projections of the distribution of regions of negative throw gradient on Faults 1 and 2. Note the sub-horizontal arrangement of some of these, as for example indicated by the arrows on Fault 1. The faults are plotted at the same scale, with no vertical exaggeration.

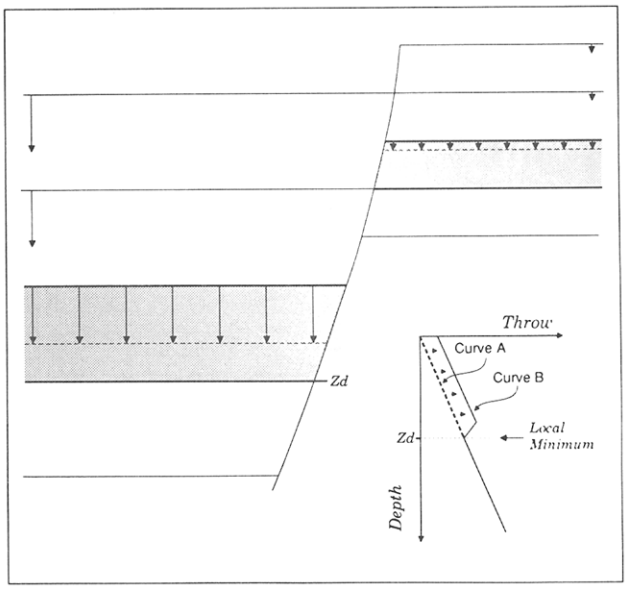

Fig. 8. Illustration depicting the effects of differential compaction on the offset of a sedimentary unit across a growth fault. A throw minimum at depth *Zd* (curve B) will automatically be generated from a previously uniform increase of displacement with depth (curve A) if the compaction in the hangingwall is sufficient to increase the throw at the top of the compacting layer to a value greater than that at its base.

1978), the maximum potential negative throw gradients that could result from the combined effects of differential compaction and changes in seismic interval velocities were calculated for the burial depth ranges associated with Faults 1 and 2 in the study area (see Appendix). Using these values as a limit by which to filter the respective negative gradient values leaves only the steeper gradients that must represent real throw minima resulting from some alternative mechanism. The recalculated plots are presented as Fig. 9 (cf. Fig. 7). Many of the smaller apparent anomalies have been filtered out and the lateral continuity of the larger ones is now much more disjointed. A number of well-defined, sub-horizontal bands of negative gradient across the fault planes nevertheless remain, which suggests they are genuine features of the distributions of throw across the faults.

DISCUSSION

The displacement mapping presented in this paper shows the pattern of throw over two growth faults to be characterized by numerous local anomalies, many of which are aligned along the fault planes to define sub-horizontal trends. These distributions are inconsistent with models of fault growth that require a systematic addition of slip across the entire fault plane at each rupture or sliding event (Watterson 1986). Neither do they conform with the sub-vertical anomalies expected for points of linkage between neighbouring normal faults interacting along strike (Childs *et al.* 1995). But, in common with patterns recorded from slip-inversions of large earthquakes, it is possible that they represent the cumulative expression of variable patterns of heterogeneous slip distribution during consecutive rupture events on the fault planes (M. Ellis personal communication). The ordered arrangement of the anomalies in sub-horizontal bands, however, points to a recurrent and systematic mechanical influence which continually impedes the distribution of slip at well-constrained regions of the fault planes. Two explanations can then be considered to account for these distributions.

Firstly, it is possible that the slip distributions are influenced by lithology, since the displacement anomalies generally trend sub-parallel to the lithological stratification where it intersects individual fault planes. Indeed, based on observations from field examples, it has been argued that fault slip distributions are strongly dependent on contrasts in material competence (Muraoka & Kamata 1983, Peacock & Zhang 1994). Therefore, displacement minima may be expected to occur wherever normal faults grow in interbedded units that have variable rheologies. In this case, they should also be expected to show a direct correlation with particular lithologies in any given setting. However, the arrangement of the recorded displacement minima at contrasting stratigraphic levels on Faults 1 and 2 suggests that lithology has not imposed a significant mechanical control on the slip distributions in this case.

Secondly, it is possible that the throw minima occur because of a decrease of displacement towards the tips of fault segments that have an overlap configuration parallel to the slip direction. A careful inspection of the seismic data in those regions of the fault planes characterized by negative throw gradients has revealed that a number of the throw minima do correlate with parts of the faults interpreted with such a configuration (Fig. 10) and as such could be considered to be analogous to jogs developed along strike-slip faults (Segall & Pollard 1980, Martel *et al.* 1988, Peacock 1991, Martel & Pollard 1993). Continuing the analogy, such configurations suggest that the en échelon segments are precursors to the development of throughgoing planes in the dip direction. The growth of these normal faults is then at least partly dictated by the upward and downward propagation, and eventual linkage, of smaller faults. This type of slip-parallel segment linkage is referred to as dip linkage, to distinguish it from the more widely discussed linkage of segments along fault strike.

One possible evolutionary sequence for segment linkage in the dip direction of a normal fault is schematically illustrated in Fig. 11. In this example, early extension is first accommodated as ductile flexuring in discrete, inclined narrow bands. Later brittle deformation (Fig. 11a) is then concentrated within these narrow zones, small slip surfaces nucleating at points of weakness in the material. Accompanying the nucleation of new faults, continued shear on these discontinuities results in growth by tip propagation at each slip event (Figs. 11b & c). Eventually, the alignment of neighbouring faults, associated with their initial nucleation positions and collinear propagation trajectories, results in overlap and relay formation. Subsequent deformation in the relay

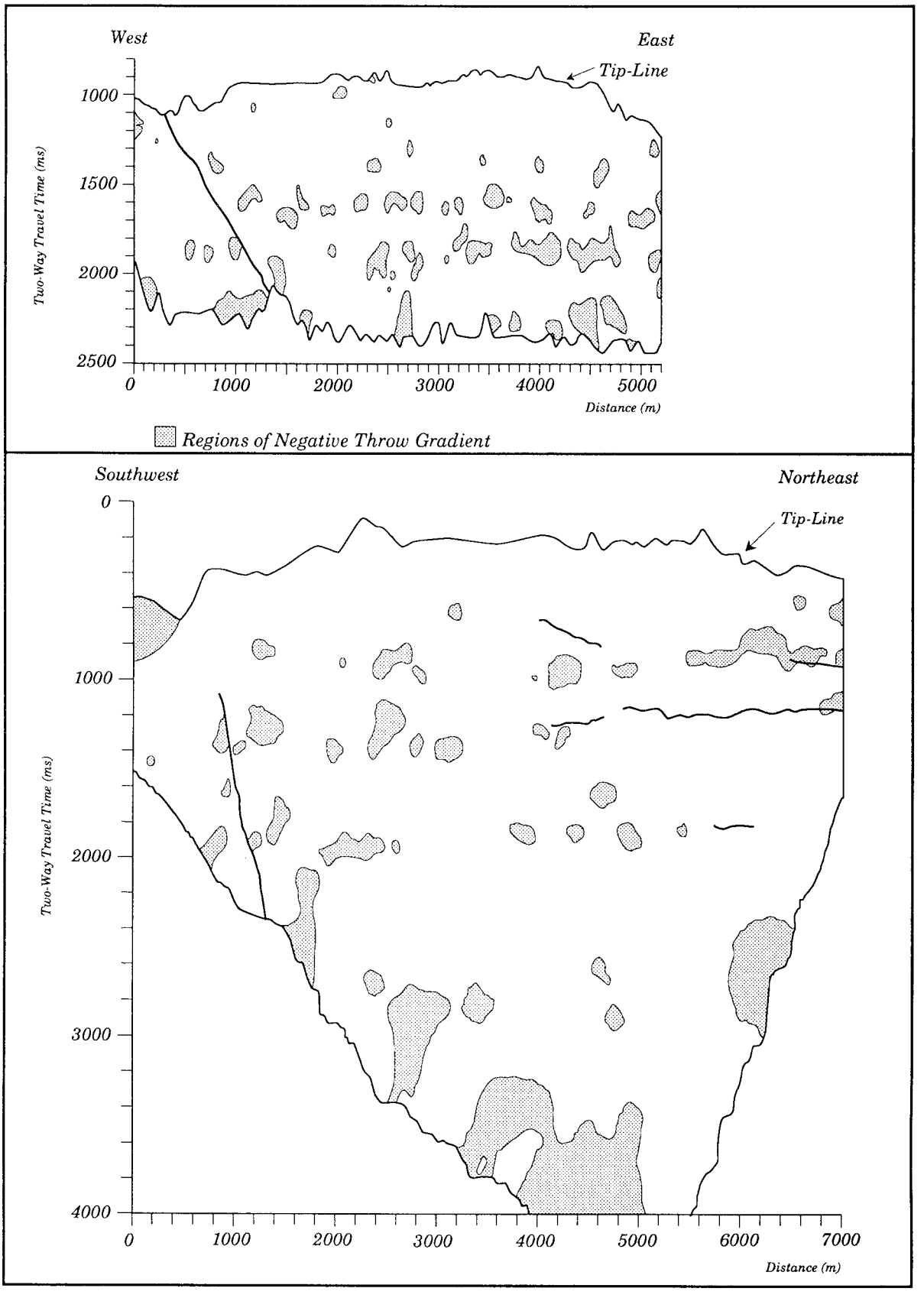

Fig. 9. Recalculated distributions of negative throw gradients on Faults 1 and 2. The potential combined contributions of differential compaction and changes in interval velocity across the faults have been removed, yet the sub-horizontal arrangements of the negative gradients are still clearly apparent. The faults are plotted at the same scale, with no vertical exaggeration.

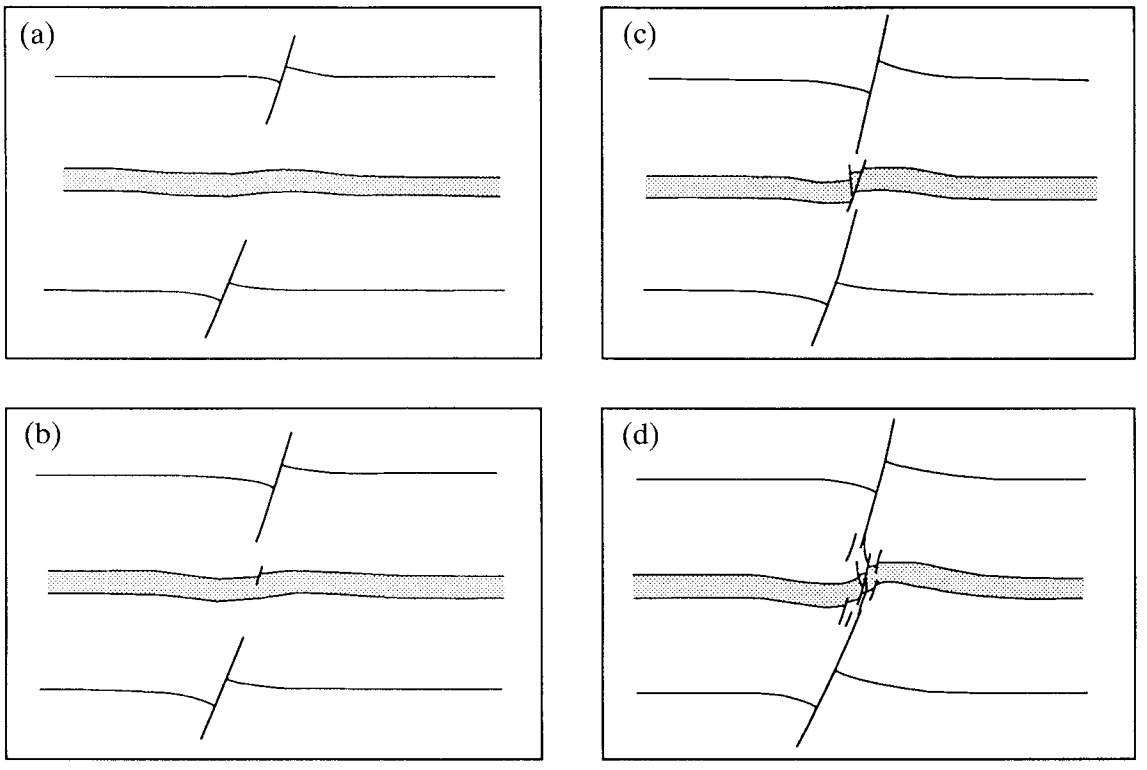

Fig. 11. Four-stage, schematic model depicting the progressive evolution of a normal fault plane from linkage in the dip direction between two initially isolated fault segments. The accumulation of displacement on initially isolated, precursor fault segments (a) results in growth by tip-line propagation (b). As the neighbouring tips approach one another a mix of brittle and ductile deformation occurs in the region between them (c) until the segments link to form a single, coherent structure (d).

structure then results in eventual linkage, to form increasingly larger slip surfaces (Fig. 11d). The overlap of faults in the dip direction produces relay structures that are elongated approximately parallel to fault strike. Since the linkage points correspond to relict fault tips and are thus associated with points of displacement minima, the corresponding displacement anomalies are similarly aligned parallel to fault strike.

Linkage between individual fault segments in the dip direction has previously been recognized as a possible evolutionary mechanism for a number of both normal and thrust faults, based principally on observations of structural styles and displacement distributions expressed in cross-sections (Laubscher 1956, Muraoka & Kamata 1983, Ellis & Dunlap 1988, Peacock & Zhang 1994). However, in this study, employing the enhanced spatial resolution of three-dimensional seismic data has allowed the geometries of the dip-direction relay zones to be mapped in detail over the fault surfaces.

The alignment of many of the throw anomalies in sub-horizontal trends that extend over the fault surfaces for many kilometres implies that the relay zones in the slip direction bound highly elliptical initial precursor fault segments that are elongated parallel to strike (Fig. 12). It has been argued that faults growing essentially in isolation are in general only slightly elliptical, with axial ratios of approximately 2 (Walsh & Watterson 1989). Therefore, a fault formed by coalescence of precursor segments with only moderate ellipticities could be expected to exhibit an arrangement of anomalies that define the segment boundaries by combinations of oblique, sub-vertical and sub-horizontal zones of throw minima (Fig. 12a). However, the almost exclusively sub-horizontal alignment of the throw anomalies in the study area suggests that Faults 1 and 2 have evolved from linkage between segments with much greater ellipticities (Fig. 12b).

It is possible to find some correspondence between topological irregularities in the seismic expression of the faults and the positions of throw anomalies. Over much of the extent of the regions of throw minima, however, there is no obvious structural expression of the evolution of dip linkage equivalent to that shown in Fig. 10. There are two possible reasons for this: (1) the structures are not resolved by the seismic data, or (2) the original dip-linkage structures have been deformed during post-linkage slip on the fault, and any original topological irregularities have been largely eliminated. Local complexities in fault topology resulting from dip-linkage structures are unlikely to be well imaged on seismic cross-sectional profiles, for finite trace spacing and limited frequency content mean that faults are not imaged as single, discrete planes, but rather as diffuse deformation zones. The width of the seismically imaged fault zone obscures the detail of important smaller structures associated with the fault. In addition, dip-linkage structures can be expected to have a very low preservation potential during continued fault slip. By comparison, branch line and relay structures on normal and thrust faults produced during the linkage of overlapping seg-

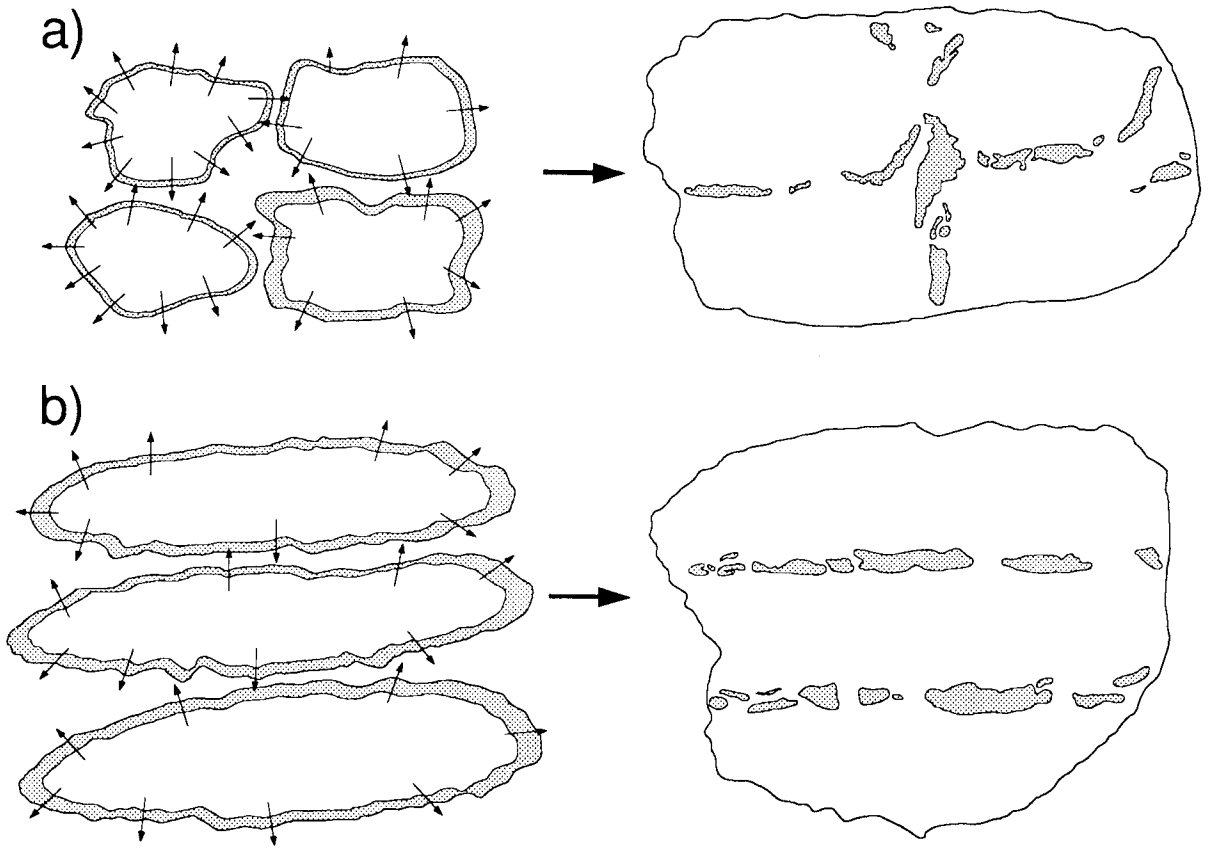

Fig. 12. Illustration showing the contrasting patterns of displacement minima expected from linkage between faults with different axial ratios. Initially isolated faults are normally expected to be only slightly elliptical (a) and linkage should therefore produce patterns of displacement minima at the relict segment boundaries that reflect this. However, the identification of predominantly sub-horizontal displacement anomalies (b) implies that the linking faults are highly elliptical, with large axial ratios sub-parallel to fault strike.

ments in the strike direction have a much higher preservation potential during continued fault slip because the topological irregularity or step on the linked fault surface is parallel to the slip direction (Scholz 1990) and is therefore more likely to be imaged by seismic data. Offsets, bends and breached relay structures create rough fault plane topologies that along the strike of normal and strike-slip faults have been known to act as barriers to earthquake rupture distribution (Tchalenko & Berberian 1975, Das & Aki 1977, Aki 1979, Sibson 1985, Crone & Haller 1991, dePolo *et al.* 1991, Machette *et al.* 1991, Zhang *et al.* 1991, Cowie & Scholz 1992). In a similar manner, dip-linkage sites might also be expected to arrest or impede slip, such that the continued partitioning of slip between relict fault segments after linkage will accentuate the displacement minima at linkage points, producing irregular displacement distributions. Consequently, whilst seismic data may be unable to resolve the structure, the mechanical influence of these structures on the local accommodation of slip will leave a strong signature in the displacement field, which can be imaged by detailed mapping of the fault displacement distribution.

CONCLUSIONS

(1) The distribution of throw across well-defined growth faults has been shown to be characterized by local displacement minima that tend to be arranged in sub-horizontal discontinuous bands across the fault planes.

(2) The resolution of these generally small anomalies is critically dependent on the sampling density used to record the displacement distribution. Maintaining a consistently high sampling density is crucial if the true spatial definition of the anomalies is to be defined.

(3) The distribution of these anomalous regions of decreasing throw is inconsistent with models of fault growth that require a systematic distribution of slip, and the sub-horizontal trend of the anomalies does not match those normally associated with relay and branch line structures of faults linked along strike. Their spatial arrangement is, however, consistent with a process of dip-linkage between elliptical fault segments with very large axial ratios, elongated sub-parallel to fault strike. Similar anomalous throw distributions across all of the faults in the survey area lead to the conclusion that growth by coalescence and linkage between small, elongated elliptical faults is probably a fundamental characteristic of the evolution of all large growth faults in this part of the Gulf of Mexico.

Acknowledgements—Thanks are due to GECO-PRAKLA for kindly providing the seismic data set upon which this work is based, and for their permission to publish the results. We would also like to express our gratitude to Michael Ellis, Emanuel Willemse and to Lidia Lonergan for their reviews and helpful criticisms, from which this manuscript has benefited considerably. C.M. is the recipient of a studentship from Shell International Petroleum Company Limited.

REFERENCES

Aki, K. 1979. Characterisation of barriers on an earthquake fault. *J. geophys. Res.* **84**, 6140–6148.

Barnett, J. A. M., Mortimer, J., Rippon, J. H., Walsh, J. J. & Watterson, J. 1987. Displacement geometry in the volume containing a single normal fault. *Bull. Am. Ass. Petrol. Geol.* **71**, 925–937.

Burgess, W. J. 1976. Geologic evolution of the mid-continent and Gulf Coast areas—a plate tectonics view. *Trans. Gulf Coast Ass. geol. Soc.* **26**, 132–143.

Chapman, T. J. & Meneilly, A. W. 1990. Fault displacement analysis in seismic exploration. *First Break* **8**, 11–22.

Chapman, T. J. & Meneilly, A. W. 1991. The displacement patterns associated with a reverse-reactivated normal growth fault. In: *The Geometry of Normal Faults* (edited by Roberts, A. M., Yielding, G. & Freeman, B.). *Spec. Publ. geol. Soc. Lond.* **56**, 183–191.

Childs, C., Easton, S. J., Vendeville, B. C., Jackson, M. P. A., Lin, S. T., Walsh, J. J. & Watterson, J. 1993. Kinematic analysis of faults in a physical model of growth faulting above a viscous salt analogue. *Tectonophysics* **228**, 313–329.

Childs, C., Watterson, J. & Walsh, J. J. 1995. Fault overlap zones within developing normal fault systems. *J. geol. Soc. Lond.* **152**, 535–549.

Clausen, O. R. & Korstgard, J. A. 1994. Displacement geometries along graben bounding faults in the Horn Graben, Offshore Denmark. *First Break* **12**, 305–315.

Cowie, P. A. & Scholz, C. H. 1992. Growth of faults by accumulation of seismic slip. *J. geophys. Res.* **97**(B7), 11,085–11,095.

Crone, A. J. & Haller, K. M. 1991. Segmentation and the coseismic behaviour of Basin and Range normal faults: examples from east-central Idaho and southwestern Montana, U.S.A. *J. Struct. Geol.* **13**, 151–164.

Das, S. & Aki, K. 1977. Fault plane with barriers: a versatile earthquake model. *J. geophys. Res.* **82**, 5658–5670.

Dawers, N. H., Anders, M. H. & Scholz, C. H. 1993. Growth of normal faults: displacement–length scaling. *Geology* **21**, 1107–1110.

dePolo, C. M., Clark, D. G., Slemmons, D. B. & Ramelli, A. R. 1991. Historical faulting in the Basin and Range province, western North America: implications for fault segmentation. *J. Struct. Geol.* **13**, 123–136.

Ellis, M. A. & Dunlap, W. J. 1988. Displacement variation along thrust faults: implications for the development of large faults. *J. Struct. Geol.* **10**, 183–192.

Freeman, B., Yielding, G. & Bradley, M. 1990. Fault correlation during seismic interpretation. *First Break* **8**, 87–95.

Jackson, M. P. A. & Galloway, W. E. 1984. Structural and depositional styles of Gulf Coast Tertiary continental margins: application to hydrocarbon exploration. *Am. Ass. Petrol Geol.* Continuing Education Course Note Series No. 25.

Laubscher, H. P. 1956. Structural and seismic deformations along normal faults in the Eastern Venezuelan Basin. *Geophysics* **21**, 368–387.

Machette, M. N., Personius, S. F., Nelson, A. R., Schwarz, D. P. & Lund, W. R. 1991. The Wasatch fault zone, Utah: segmentation and history of Holocene earthquakes. *J. Struct. Geol.* **13**, 137–149.

Magara, K. 1978. *Compaction and Fluid Migration. Practical Petroleum Geology.* (Development in Petroleum Science; 9). Elsevier, Amsterdam.

Martel, S. J. & Pollard, D. D. 1993. Mechanics of slip and fracture along small faults and simple strike slip fault zones in granitic rock. *J. geophys. Res.* **94**, 9417–9428.

Martel, S. J., Pollard, D. D. & Segall, P. 1988. Development of simple strike-slip fault zones, Mount Abott Quadrangle, Sierra Nevada, California. *Bull. geol. Soc. Am.* **100**, 1451–1465.

Muraoka, H. & Kamata, H. 1983. Displacement distribution along minor fault traces. *J. Struct. Geol.* **5**, 483–495.

Murray, G. E. 1951. Sedimentary volumes in Gulf Coastal plain of the United States and Mexico. Part 3: Volume of Mesozoic and Cenozoic sediments in central Gulf Coastal plain of the United States. *Bull. geol. Soc. Am.* **63**, 1177–1192.

Peacock, D. C. P. 1991. Displacements and segmental linkage in strike-slip fault zones. *J. Struct. Geol.* **13**, 1025–1035.

Peacock, D. C. P. & Sanderson, D. J. 1991. Displacements, segment linkage and relay ramps in normal fault zones. *J. Struct. Geol.* **13**, 721–733.

Peacock, D. C. P. & Sanderson, D. J. 1994. Geometry and development of relay ramps in normal fault systems. *Am. Ass. Petrol. Geol. Bull.* **78**, 147–165.

Peacock, D. C. P. & Zhang, X. 1994. Field examples and numerical modelling of oversteps and bends along normal faults in cross-section. *Tectonophysics* **234**, 147–167.

Petersen, K., Clausen, O. R. & Korstgard, J. A. 1992. Evolution of a salt-related listric growth fault near the D-1 well, block 5605, Danish North Sea: displacement history and salt kinematics. *J. Struct. Geol.* **14**, 565–577.

Reymond, B. A. & Stampfli, G. M. 1994. Sequence stratigraphic interpreation of 3D seismic data offshore Louisiana—a case study. *First Break* **12**, 453–462.

Rippon, J. H. 1985. Contoured patterns of the throw and hade of normal faults in the Coal Measures (Westphalian) of north-east Derbyshire. *Proc. Yorks. geol. Soc.* **45**, 147–161.

Scholz, C. H. 1990. *Mechanics of Faulting and Earthquakes.* Cambridge University Press, Cambridge.

Scholz, C. H., Dawers, N. H., Yu, J.-Z., Anders, M. H. & Cowie, P. A. 1993. Fault growth and fault scaling laws: preliminary results. *J. geophys. Res.* **98**, 21951–21961.

Segall, P. & Pollard, D. D. 1980. Mechanics of discontinuous faults. *J. geophys. Res.* **85**(B8), 4337–4350.

Sibson, R. H. 1985. Stopping of earthquake ruptures at dilational fault jogs. *Nature* **316**, 248–251.

Tchelenko, J. S. & Berberian, M. 1975. Dasht-e-Bayez fault, Iran: earthquake and earlier related structures in bedrock. *Bull. geol. Soc. Am.* **86**, 703–709.

Thorsen, C. E. 1963. Age of growth faulting in southeast Louisiana. *Trans. Gulf Coast Ass. geol. Soc.* **13**, 103–110.

Trudgill, B. D. & Cartwright, J. A. 1994. Relay ramp forms and normal fault linkages—Canyonlands National Park, Utah. *Bull. geol. Soc. Am.* **106**, 1143–1157.

Walsh, J. J. & Watterson, J. 1987. Distribution of cumulative displacement and seismic slip on a single normal fault surface. *J. Struct. Geol.* **9**, 1039–1046.

Walsh, J. J. & Watterson, J. 1988. Analysis of the relationship between displacements and dimensions of faults. *J. Struct. Geol.* **10**, 239–247.

Walsh, J. J. & Watterson, J. 1989. Displacement gradients on fault surfaces. *J. Struct. Geol.* **11**, 307–316.

Walsh, J. J. & Watterson, J. 1990. New methods of fault projection for coalmine planning. *Proc. Yorks. geol. Soc.* **48**, 209–219.

Walsh, J. J. & Watterson, J. 1991. Geometric and kinematic coherence and scale effects in normal fault systems. In: *The Geometry of Normal Faults* (edited by Roberts, A. M., Yielding, G. & Freeman, B.). *Spec. Publ. geol. Soc. Lond.* **56**, 193–203.

Watterson, J. 1986. Fault dimensions, displacements and growth. *Pure & Appl. Geophys.* **124**, 365–373.

Zhang, P., Slemmons, D. B. & Mao, F. 1991. Geometric pattern, rupture termination and fault segmentation of the Dixie Valley–Pleasant Valley normal fault system, Nevada, U.S.A. *J. Struct. Geol.* **13**, 165–176.

APPENDIX

Consider a sedimentary sequence across a fault having an upper and lower bound defined by horizons at which measurements of throw have been made (Fig. A1). If the thicknesses, the interval velocities and the measured OWTTs associated with this sequence are defined as in the figure, then the throw gradient m, between the sample points is given by:

$$m = \frac{(t_4 - t_3) - (t_2 - t_1)}{\left(t_3 + \left(\frac{t_4 - t_3}{2}\right)\right) - \left(t_1 + \left(\frac{t_2 - t_1}{2}\right)\right)} = \frac{2(t_4 - t_3 - t_2 + t_1)}{t_4 + t_3 - t_2 - t_1}. \quad \text{(A1)}$$

But $t_4 = t_2 + (D_2/V_2)$ and $t_3 = t_1 + (D_1/V_1)$, so

$$m = \frac{2\left(\frac{D_2}{V_2} - \frac{D_1}{V_1}\right)}{\frac{D_2}{V_2} + \frac{D_1}{V_1}}. \quad \text{(A2)}$$

Therefore,

$$\frac{D_2}{D_1}(2 - m) = \frac{V_2}{V_1}(2 + m). \quad \text{(A3)}$$

The above relationship determines that a negative throw gradient across a fault will be apparent in the seismic data if the ratio of thicknesses, D_2/D_1 is smaller than the ratio of interval velocities V_2/V_1.

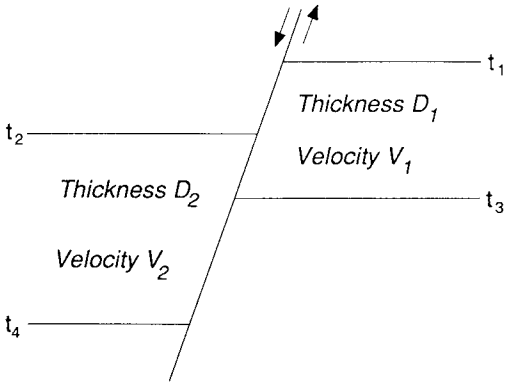

Fig. A1. Hypothetical displaced sequence of sedimentary units whose upper and lower bounds are defined by the points at which measurements of fault throw are recorded. Calculations of throw gradient are based upon the bulk values of thickness, D, and interval velocity, V, that characterize each of the displaced sequences between the sampling points. Travel times, t, are in ms OWTT, and throw gradient, m, is dimensionless (ms/ms). See text for details.

Lithological changes, in particular, are therefore likely to introduce considerable variability into recorded displacement gradients. For the case of Faults 1 and 2 in the study area, it is reasonable to infer that lithological changes are not associated with the generally low average expansion ratios (≈1.1). Lithological changes may possibly occur over the limited stratigraphic intervals, where expansion ratios are highest (≈2.7).

Assuming a general case of no lithological changes, then for the maximum differential burial depths across Fault 1, i.e. at a throw of 100 m, burial curves estimate approximately 0.2% differential compaction. Taking this to have all been accommodated as vertical shortening, this means that D_2 is 99.8% of D_1. With a value of V_2 no more than 5% greater than V_1, i.e. due to its deeper burial, V_2 is 105% of V_1, then the maximum negative throw gradient that could be produced from a combination of both velocity and compaction variations across Fault 1 is given by:

$$0.998(2 - m) = 1.05(2 + m), \text{ or } m = -0.051. \quad \text{(A4)}$$

Due to the greater vertical extent of Fault 2 and the consequently larger variations in compaction and velocities that can be expected over this range, the limiting negative throw gradient was calculated over two depth intervals. At depths less than 2000 ms TWTT, the above values were used, as here the fault has comparable displacements to those of Fault 1. Below 2000 ms TWTT, D_2 was calculated to be 99.9% of D_1 and V_2 was taken to be 10% greater than V_1, giving a value for m of −0.096.

The same relationship predicts that where the expansion ratios are a maximum, a negative throw gradient will not result, even when differing lithologies with sharply contrasting compaction characteristics, such as overpressured sandstone in the footwall and shale in the more deeply buried hangingwall, are assumed. This is because the thicker hangingwall units require even greater differential compaction in order for a throw minimum to result, and since the throw at any point across the faults in the survey area is only ever a small fraction of the burial depths, then the effects of differential compaction are almost negligible. However, in settings outside the survey area where much larger expansion ratios exist, then the effects of differential compaction can be expected to be much greater, and consequently a ratio of thicknesses smaller than the ratio of velocities may obtain particularly in the near surface, where the rates of compaction and velocity change are greatest (Magara 1978).